1 # Source attribution of near-surface ozone trends in the United States during 1995–2019

6 Pengwei Li[1], Yang Yang[1*], Hailong Wang[2], Su Li[1], Ke Li[1], Pinya Wang[1], Baojie

7 Li[1], Hong Liao[1]

10 [1]Jiangsu Key Laboratory of Atmospheric Environment Monitoring and

11 Pollution Control, Jiangsu Collaborative Innovation Center of Atmospheric

12 Environment and Equipment Technology, School of Environmental Science

13 and Engineering, Nanjing University of Information Science and Technology,

14 Nanjing, Jiangsu, China

15 [2]Atmospheric Sciences and Global Change Division, Pacific Northwest

16 National Laboratory, Richland, Washington, USA

20 *Correspondence to yang.yang@nuist.edu.cn

Abstract

Emissions of ozone (O_3) precursors in the United States have decreased in recent decades, and near-surface O_3 concentrations showed a significant decrease in summer but an increase in winter. In this study, an O_3 source tagging technique is utilized in a chemistry-climate model to investigate the source contributions to O_3 mixing ratios in the U.S. from various emitting sectors and regions of nitrogen oxides (NO_x) and reactive carbon species during 1995–2019. We show that domestic emission reductions from energy and surface transportation are primarily responsible for the decrease in summertime O_3 during 1995–2019. However, in winter, the emission control also weakens the NO_x titration process, resulting in considerable increases in O_3 levels from natural sources. Additionally, increases in aviation and shipping emissions and transpacific transport of O_3 from Asia largely contribute to the winter O_3 increase. We also found that changes in large-scale circulation favoring O_3 transport from upper atmosphere and foreign transport from Asia also explain 15% of the increase in the U.S. near-surface O_3 levels in winter.

1. Introduction

Ozone (O_3) near the surface has a significant impact on air quality and public health (Haagen-Smit, 1952; Fleming et al., 2018). Since the increase in anthropogenic emissions of O_3 precursors from preindustrial times, O_3 has now become the third most important anthropogenic greenhouse gas in the troposphere (Myhre et al., 2013). Major sources of O_3 in the troposphere include the transport from the stratosphere and formation through photochemical reactions within the troposphere involving two chemically distinct groups of precursors: nitrogen oxides (NO_x) and reactive carbon species, including carbon monoxide (CO), methane (CH_4), and non-methane volatile organic compounds (NMVOCs) (Atkinson, 2000). O_3 precursors come from a variety of sectors, and its relatively long lifetime of about 22 days (Stevenson et al. 2006) favors the long-range transport of O_3. Due to the nonlinearity of the O_3 production and its associated dependence on precursor emissions (Seinfeld and Pandis, 2006), attributing O_3 pollution to its sources is complicated.

Since the 1980s, O_3 precursor emissions have significantly reduced in the United States (Duncan et al., 2016; Xing et al., 2013; Zhang et al., 2016; Zhang et al., 2021). However, due to the nonlinear production chemistry of O_3, complex seasonal meteorological influence, and long-range transport from foreign source regions, domestic emissions reductions do not imply a decrease in seasonal and annual O_3 concentrations. According to remote surface measurements (Cooper et al., 2020) and aircraft observations (Gaudel et al., 2020), the Sixth Assessment Report of the Intergovernmental Panel on Climate Change (Szopa et al., 2021) showed a decreasing trend in annual mean O_3 concentrations in the western U.S. but an increasing trend in the eastern U.S. since the mid-1990s. On the seasonal timescale, surface observations and modeling results showed that O_3 concentrations over the U.S. had decreased

65   in summer due to the reductions in domestic anthropogenic emissions and

66   increased in winter related to the weakened NO_x titration since the late 1980s

67   (Cooper et al., 2012; Lin et al., 2017). It also shows that the increased

68   background O_3, especially due to an increased transport from Asia, can partly

69   offset the benefit of domestic emissions control over the western U.S. in

70   summer.

71   Source apportionment is a useful method for quantifying contributions to

72   air pollutants from specific source regions and/or sectors, which is beneficial to

73   emission control strategies (Yang et al., 2018). One method of obtaining an O_3

74   source-receptor relationship is to zero out or perturb emissions from a given

75   source region or sector in sensitivity simulations along with a baseline

76   simulation, which gives information about the response of O_3 to changes in

77   precursor emissions (e.g., Fiore et al., 2009; Hoor et al., 2009). However,

78   emission perturbation method requires many additional model simulations

79   when being used to estimate the impacts of changes in multiple sources (Koo

80   et al., 2009; Wang et al., 2014). The perturbation method may invalidate the

81   assumption of a linear relationship between the magnitude of the emission

82   perturbation and the magnitude of the O_3 change considering the nonlinearity

83   in O_3 chemistry, especially if large perturbations (e.g. zeroing out regional or

84   sector-wide emissions) are used. The tagging approach produces information

85   about the contribution of precursor emissions to the total amount of O_3 (Butler

86   et al., 2020). The perturbation and tagging methods are two different methods

87   answering different scientific questions, with the first for the impacts and the

88   last for the contributions (Grewe et al. 2010, Emmons et al. 2012, Clappier et

89   al. 2017 and Thunis et al., 2019). Both of these two methods can be used for

90   specific purpose to provide a comprehensive understanding of source-receptor

91   relationships between precursor emissions and O_3 concentrations.

92   The source tagging method has been widely adopted in regional air quality

93   models to examine the O_3 attribution in the U.S., China, and/or Europe (Gao et

94   al., 2016; Collet et al., 2018; Lupaşcu and Butler, 2019). In some regional

95   models, O_3 apportionment is based on the ratio of chemical indicators to

96   determine the regime of O_3 generation (e.g., VOC-limited or NO_x-limited

97   regimes) and then attribute the generation of O_3 to the tag carried by a certain

98   precursor (VOCs or NO_x), which however cannot simultaneously attribute O_3

99   production to NO_x and VOCs, respectively (Dunker et al., 2002; Kwok et al.,

100 2015), while some models do not use the chemical indicators (Lupaşcu and

101 Butler, 2019; Mertens et al., 2020). In addition, due to the limitation in domain

102 size of regional air quality models, they are difficult to account for contributions

103 of intercontinental transport from several sources outside the model domain.

104 Recently, O_3 tagging techniques have been implemented in the global models

105 (e.g., Sudo and Akimoto, et al., 2007; Zhang et al., 2008; Emmons et al., 2012;

106 Grewe et al. 2017; Butler et al., 2018; Han et al., 2018; Bates and Jacob, 2020).

107 However, in many global models, O_3 is tagged by the production regions rather

108 than the precursor emission regions, so that O_3 can only be attributed to the

109 area where O_3 is generated, rather than the source of precursor emissions.

110   Here, based on a state-of-the-art tagging system implementation in a

111 global chemistry–climate model, the trends of near-surface O_3 mixing ratios in

112 the U.S. during 1995–2019 and the source attributions of the O_3 variations to

113 various emission sectors and regions of NO_x and reactive carbon species are

114 investigated in this study. Mechanisms of explaining the O_3 trends that involve

115 changes in anthropogenic emissions and large-scale circulations are also

116 explored.

117 **2. Methods**

118 **2.1 Model Description**

119   Tropospheric O_3 mixing ratios are simulated using the Community

120 Atmosphere Model version 4 with Chemistry (CAM4-chem) (Lamarque et al.,

121 2012; Tilmes et al., 2015), which is the atmospheric chemistry component of

122 the Community Earth System Model (CESM), at a horizontal resolution of 1.9°

123 latitude by 2.5° longitude with 26 vertical levels extending to 40 km above the

124 surface. The height of bottom layer is about 120 m and there are about 4 layers

125 under 2 km. The model configuration uses a comprehensive tropospheric

126 chemistry mechanism based on the Model for Ozone and Related chemical

127 Tracers version 4 (MOZART-4) (Emmons et al., 2010, 2012). Model

128 configurations simulate wet deposition of gas species using the Neu and

129 Prather (2011) scheme. Dry deposition is represented following the resistance

130 approach originally described in Wesely (1989). Stratosphere-troposphere

131 exchange of O_3 is treated by setting O_3 to stratospheric values as their

132 climatological means over 1996–2005 at the tropopause (Lamarque et al.,

133 2012), which is affected by atmospheric circulation and experiences the same

134 loss rates as O_3 in the troposphere (Tilmes et al., 2016). Sea surface

135 temperatures and sea ice concentrations in our simulations are prescribed at

136 present-day climatological conditions. The zonal and meridional wind fields are

137 nudged towards the MERRA-2 (Modern Era Retrospective-Analysis for

138 Research and Applications Version 2) reanalysis (Gelaro et al., 2017) at a 6-

139 hourly relaxation timescale in this study to better constrain large-scale

140 circulations by observations. The CAM4-chem performance in simulating

141 tropospheric O_3 and precursors has been fully evaluated in Tilmes et al. (2015).

142 **2.2 Ozone Source Tagging Technique**

143   The novel O_3 source tagging technique implemented in the model was

144 developed by Butler et al. (2018), which can provide a separate source

145 apportionment of tropospheric O_3 to the two distinct groups of precursor

146 emissions, i.e., NO_x and reactive carbon (CO, CH_4 and NMVOCs). The portion

147 of tropospheric O_3 that is attributable to the stratosphere-troposphere exchange

148 can also be quantified using this unique tagging technique. The source

149 attribution of O_3 requires two separate model runs with the tagging applied to
150 NO_x and reactive carbon species, respectively. Details of the O_3 tagging
151 technique are described in Butler et al. (2018).

152 In this study, near-surface O_3 is attributed to emission sectors and regions.
153 Emissions from individual sectors, including agriculture (AGR), energy (ENE),
154 industry (IND), residential, commercial and other (RCO), surface transportation
155 (TRA), waste management (WST), international shipping (SHP) and biomass
156 burning (BMB) emissions, as well as chemical production in the stratosphere
157 (STR) and extra chemical production (XTR, a small amount of O_3 produced due
158 to the self-reaction of OH radicals and the reactions of HO_2 with certain organic
159 peroxy radicals) are tagged for both NO_x and reactive carbon species. Aircraft
160 (AIR), soil (SOIL) and lightning (LGT) sources are separately tagged for NO_x
161 emissions, while solvents (SLV) and biogenic (BIO) sources are separately
162 tagged for NMVOCs emissions.

163 For the regional source attribution, we separately tag anthropogenic
164 sources from Africa (AFR), Central America (CAM), Europe (EUR), Middle East
165 (MDE), North America (NAM), East Asia (EAS), South Asia (SAS), Southeast
166 Asia (SEA) and rest of the world (ROW) (see Fig. 1 for the region map) and
167 natural sources (BMB, SOIL, LGT, BIO, STR and XTR). Additional tags for
168 methane (CH_4) and carbon monoxide (CO) are applied in both of the reactive
169 carbon tagging simulations that are used to attribute O_3 to emission sectors and
170 regions. We do not tag CH_4 by individual sources and the contributions of CH_4
171 from various sources are lumped in this study. It is because CH_4 has a relative
172 long lifetime in the troposphere and it is well mixed in the troposphere due to its
173 exceptionally low reactivity, which can contribute to O_3 formation at any location
174 in the troposphere where photochemical conditions are favorable (Fiore et al.,
175 2008). CO also has a longer lifetime and lower reactivity than most NMVOCs.
176 The lumped CO is tagged in the simulations for emission sectors, but not

177　specifically tagged in the simulations for emission regions due to the

178　computational limit.

179　**2.3 Emissions and Observation**

180　The global anthropogenic emissions, including NO_x, CO, NMVOCs, SO_2,

181　and NH_3, over 1990–2019 are from the Community Emissions Data System

182　(CEDS) version 20210205 (Hoesly et al., 2018) (See Table S1 and Figs. S1–

183　S3). Biomass burning emissions are obtained from the CMIP6 (Coupled Model

184　Intercomparison Project Phase 6) over 1990–2014 (van Marle et al., 2017) and

185　the emissions for the following five years (2015–2019) are interpolated from the

186　SSP2-4.5 forcing scenario (O'Neill et al., 2016). NO_x emitted from soils and

187　biogenic NMVOCs from vegetation are prescribed as in Tilmes et al. (2015) and

188　are kept at the present-day (2000) climatological levels during simulations.

189　Lightning emissions of NO_x are estimated online using the parameterization

190　based on simulated cloud top heights from Price et al. (1997), which is scaled

191　to provide a global annual emission of 3–5 Tg N yr^{-1} (Lamarque et. al., 2012).

192　CH_4 is fixed at a global average level of 1760 parts per billion (ppb, volume ratio

193　in this study) during simulations.

194　Many studies have reported that the previous CEDS version 20160726

195　(hereafter $CEDS_{2016}$) has large biases in the regional emission estimates (e.g.,

196　Cheng et al., 2021; Fan et al., 2018). In this study, the CEDS version 20210205

197　is used (hereafter $CEDS_{2021}$), which builds on the extension of the CEDS

198　system described in McDuffie et al. (2020) and extends the anthropogenic

199　emissions to year 2019. It updates country-level emission inventories for North

200　America, Europe and China and has considered the significant emission

201　reductions in China since the clean air actions in recent years. The global total

202　NO_x emission from $CEDS_{2021}$ is lower than that of $CEDS_{2016}$ after 2006 and it

203　shows a fast decline since then. In 2014, the global total anthropogenic

204　emission of NO_x in $CEDS_{2021}$ is about 10% lower than the $CEDS_{2016}$ estimate.

205   This difference is mainly reflected in the NO_x emissions in China and India.

206     $CEDS_{2021}$ has a lower estimate of the global NMVOCs emission than $CEDS_{2016}$

207   by more than 10% during the recent decades, attributed to lower emissions

208   from Africa, Central and South America, the Middle East and India. The using

209   of the $CEDS_{2021}$ emission inventory in this study could reduce the contributions

210   of NO_x emissions from East Asia and South Asia to the U.S. O_3 mixing ratios

211   and trends, as compared to $CEDS_{2016}$. However, recent study reported a

212   difference in aviation emission distribution of NO_x between CMIP5 and CMIP6

213   related to an error in data pre-processing in CEDS, leading to a northward shift

214   of O_3 burden in CMIP6 (Thor et al., 2023). Therefore, the contribution of the

215   aircraft emissions of NO_x to the O_3 mixing ratios could be overestimated at high

216   latitude regions.

217   Surface O_3 measurements in the U.S. are obtained from the U.S.

218   Environmental Protection Agency (EPA). Linear trends of surface O_3 are

219   calculated separately for boreal summer (June-July-August, JJA) and winter

220   (December-January-February, DJF). Seasonal mean for any site that has less

221   than 50% data availability in any month of a season is discarded following Lin

222   et al. (2017). O_3 trends is calculated only when the seasonal data availability is

223   greater than 85% during the analyzed period (more than 22 years). Trends in

224   this study are calculated based on the linear least-squares regressions and the

225   statistical significance is identified through the F test with the 95% confidence

226   level.

227   **2.4 Experimental Design**

228   In this study, four groups of experiments are conducted, each group

229   includes both NO_x tagging simulation and reactive carbon tagging simulation.

230   Two BASE experiment groups include simulations with emission sectors and

231   regions, respectively, tagged for the two chemical distinct precursors. The

232   BASE experiments are performed with time-varying anthropogenic emissions

233   and winds nudged to MERRA-2 reanalysis. The other two groups of sensitivity

234   experiments (MET) are the same as BASE experiments, except that the

235   anthropogenic emissions are held at year 2019 level during simulations. All

236   experiments are performed over 1990–2019, with the first 5 years treated as

237   model spin-up and the last 25 years used for analysis. The BASE experiments

238   are analyzed to quantify the source attributions of O_3 in the U.S., unless stated

239   otherwise. We note that although the wind fields are nudged at a 6-hourly

240   relaxation timescale, the atmospheric dynamics could also be slightly different

241   between simulations, leading to the slight changes in the contributions from the

242   same tags between simulations.

243   **2.5 Model Evaluation**

244   Figure 2 compares the simulated near-surface O_3 mixing ratios with those

245   from observations in 1995 and 2019, respectively. In general, the model

246   overestimates O_3 mixing ratios in the U.S. in both summer and winter by 10–

247   40%. It can capture the seasonal pattern of O_3 that high mixing ratios in summer

248   and low mixing ratios in winter. The spatial distributions can also be roughly

249   captured by the model, with statistically significant correlation coefficients

250   between simulations and observations in the range of 0.21–0.45. From 1995 to

251   2019, the O_3 mixing ratios in the U.S. decreased in summer and increased in

252   winter presented in observations. The model can produce the sign of the

253   changes, but has large biases in magnitudes, which will be discussed in the

254   following section.

255

256   **3 Results**

257   **3.1 Ground-level ozone trends in the U.S.**

258   Emissions of O_3 precursors have substantially reduced since 1995 in both

259   the western U.S. (WUS, 100–125°W, 30–45°N) and eastern U.S. (EUS, 70–

260   100°W, 30–45°N), primarily owning to the reductions in anthropogenic

261 emissions (Figs. S1–S3). However, the simulated annual near-surface O_3

262 mixing ratios present opposite trends between WUS and EUS, with increases

263 in EUS but weak decreases in WUS, which also exist in observations (Fig. 3a).

264 The simulated contrasting trends in annual mean O_3 mixing ratios between

265 the WUS and EUS are dominated by the strong decreases in O_3 mixing ratios

266 in summer across the U.S. (Fig. 3b) and increased O_3 levels in winter over the

267 central-eastern U.S. during 1995–2019 (Fig. 3c). The opposite trends between

268 summer and winter have also been noted in many previous studies (e.g.,

269 Copper et al., 2012; Lin et al., 2017, Jaffe et al., 2018). The model reproduces

270 the observed O_3 trend over EUS in summer and roughly captures the O_3 trend

271 over WUS in winter (Table 1). The decreasing trend over WUS in summer and

272 increasing trend over EUS in winter, however, are largely overestimated in the

273 model, partly attributed to the coarse model resolution. The model also tends

274 to overestimate the weakening of NO_x titration in winter, leading to the biases.

275 For spring and autumn, they are the transition between summer and winter,

276 having the similar spatial pattern of O_3 trends as annual average, and will not

277 be concerned in this study.

278 **3.2 Source attribution of ozone trends to emission sectors**

279 During 1995–2019, summer and winter NO_x emissions from energy and

280 surface transport sectors have significantly decreased in both WUS and EUS,

281 followed by industry and residential sectors, while those from aircraft have

282 increased slightly (Fig. 4). Emissions of NMVOCs from surface transportation,

283 solvents, industry, residential and waste sectors have decreased across the

284 U.S., while those from energy and agriculture have increased. CO emissions

285 have also significantly decreased over this time period.

286 The time series of the source sector contributions to O_3 mixing ratios from

287 NO_x and reactive carbon emissions are shown in Fig. 5 and the O_3 trends in the

288 U.S. attributed to different emission source sectors are shown in Fig. 6. In

289   summer, the O_3 attributed to NO_x emissions from energy and surface

290   transportation decreased at the rate of 2.0±0.2 and 1.6±0.2 ppb/decade in WUS

291   and 3.2±0.2 and 1.7±0.2 ppb/decade in EUS, respectively (Figs. 6a and 6c).

292   On the contrary, the O_3 contributed by aircraft NO_x emissions increased by 0.4

293     $\pm$ 0.0 ppb/decade in both WUS and EUS. Along with the reductions in

294   anthropogenic emissions, natural emissions are becoming increasingly

295   important as sources for O_3 formation near the surface. Although NO_x

296   emissions from soil are held at the present-day climatological levels, they

297   account for 0.7±0.1 and 1.7±0.1 ppb/decade increase in WUS and EUS,

298   respectively, during 1995–2019, related to the changing O_3 production

299   efficiency under the more NO_x-sensitive condition. Note that, during 1995–2019,

300   the molar ratio (mol N /mol C) of emitted NO_x to NMVOCs reduced from 0.11 to

301   0.07 in WUS and from 0.14 to 0.07 in EUS, confirming the enhanced NO_x-

302   sensitive condition during the analyzed time period. In recent decades, global

303   emissions from international shipping have increased rapidly (Eyring et al.,

304   2005; Müller-Casseres et al., 2021), but have declined near the coast of the

305   United States. Due to a strong chemical sink associated with photolysis of O_3

306   with subsequent production of hydroxyl radical (OH) from water vapor in

307   summer (Johnson et al., 1999), the effect of increased international shipping

308   emissions over the remote ocean regions on the continental U.S. was blunted.

309   But the increase in shipping emissions inland tends to increase O_3 mixing ratios

310   in eastern U.S. (Fig. S4).

311   In summer, biogenic sources dominate the emissions of NMVOCs in the

312   U.S. (Fig. S3). As the O_3 decreases, mainly due to the reductions in domestic

313   NO_x emissions, the contributions from biogenic emissions of NMVOCs have a

314   decreasing trend in the U.S. during 1995–2019 (Figs. 6b and 6d), even though

315   biogenic emissions were fixed during simulations. This also applies to CH_4, of

316   which the mixing ratio was kept constant. This does not actually mean that CH_4

317   and biogenic NMVOCs themselves contributed to the overall O_3 trend through

318   changing the precursor levels since they were kept constant during simulations;

319   rather, mainly due to the reductions in NO_x emissions, O_3 production efficiency

320   by reactive carbon species decreases, leading to decreasing trends of O_3

321   contribution by CH_4 and biogenic NMVOCs. In conjunction with NO_x emission

322   reductions, decreases in NMVOCs emissions from surface transportation and

323   industry sectors contribute negative O_3 trends of −0.3±0.0 and −0.1±0.0

324   ppb/decade, respectively, in both WUS and EUS in summer (Figs 6b and 6d),

325   which are offset by the increases in NMVOCs emissions from energy and

326   agriculture sectors. Although the O_3 production efficiency of CO is relatively low,

327   the contributions of CO to O_3 mixing ratios largely decreased with trends of −

328   0.6±0.1 and −0.5±0.1 ppb/decade in WUS and EUS, respectively, due to the

329   massive reduction in anthropogenic emissions of CO (Fig. S1).

330   In winter, through the weakened NO_x titration process (Gao et al., 2013;

331   Simon et al., 2015), the NO_x emission control causes an increase in O_3 levels

332   during 1995–2019, especially the contribution from surface transportation

333   (0.4±0.0 ppb/decade in WUS and 0.8±0.1 ppb/decade in EUS) (Figs. 6e and

334   6g). Although aircraft NO_x emissions slightly increased, O_3 attributed to aircraft

335   NO_x emissions shows positive trends as large as 0.4±0.0 and 0.6±0.0

336   ppb/decade in WUS and EUS, respectively. It is because aircraft emissions are

337   injected directly into the upper troposphere and lower stratosphere in a low

338   ambient NO_x condition and have a much higher O_3 enhancement efficiency

339   than surface emissions (Hodnebrog et al., 2011). It can be confirmed that the

340   NO_x from aircraft contributes to the increase in O_3 mixing ratios at 250 hPa in

341   high latitude regions of the Northern Hemisphere during 1995–2019 (Fig. S5).

342   The decrease in near-shore shipping emissions weakened the NO_x titration,

343   together with the weakened O_3 chemical sink from water vapor in winter,

344   leading to large increasing trends of O_3 by 0.8±0.1 and 1.0±0.1 ppb/decade,

345 respectively, in the WUS and EUS during 1995–2019. Although most natural

346 emissions do not change during the simulations, the net O_3 chemical production

347 is more sensitive to NO_x under the emission control condition, resulting in the

348 increasing O_3 trends contributed by the soil and lightning NO_x emissions. Due

349 to the weakened NO_x titration in winter, the contribution of stratospheric

350 intrusion increases at a rate of 0.6±0.1 and 1.0±0.1 ppb/decade over WUS and

351 EUS, respectively, when stratospheric contribution to the near-surface O_3 is

352 relatively high (Butler et al., 2018). Along with the weakened NO_x titration,

353 contributions from reactive carbon emissions to the near-surface O_3 in the U.S.

354 also increase for most species and sectors (Figs. 6f and 6h).

355 **3.3 Source attribution of ozone trends to emission regions**

356   Time series of the source region contributions to near-surface O_3 mixing

357 ratios are shown in Fig. 7 and the O_3 trends in the U.S. attributed to different

358 emission source regions are presented in Fig. 8. In summer, domestic

359 anthropogenic NO_x emissions (excluding those from soil) within North America

360 account for 49% of the near-surface O_3 mixing ratio averaged over the U.S.

361 (WUS+EUS) in 1995–2019. The domestic emission reduction is the dominant

362 factor causing the decline in surface O_3 mixing ratios, with contributions of –

363 4.4±0.2 and –5.7±0.3 ppb/decade to the trends over WUS and EUS,

364 respectively, during 1995–2019 (Figs. 8a and 8c). Reductions in the NMVOCs

365 emissions from North American anthropogenic sources also decrease O_3

366 mixing ratios (Figs. 8b and 8d), accompanying with the domestic NO_x emission

367 control. The increase in NO_x emissions from Asia contributes 0.7±0.1

368 ppb/decade to the total O_3 increasing trend in WUS, partly offsetting the

369 negative impact of domestic emission reductions, but has a weak impact in EUS,

370 which is consistent with previous studies (Lin et al., 2017).

371   In winter, domestic anthropogenic NO_x emissions only account for 19% of

372 the surface O_3 mixing ratio in the U.S. over 1995–2019, while NO_x sources from

373   lightning, rest of the world (mainly from the international shipping), and Asia

374   contribute 17%, 14%, and 11%, respectively. O_3 from stratospheric intrusion

375   contributes 21% of the near-surface O_3 in the U.S. in winter. During 1995–2019,

376   the significant increase in wintertime surface O_3 mixing ratios are not directly

377   linked to the reductions in domestic anthropogenic emissions (Figs. 8e and 8g).

378   However, the domestic emission control weakens the NO_x titration, resulting in

379   considerable increases in O_3 originating from the natural sources, including O_3

380   from stratospheric intrusion, lightning and soil emissions. The natural sources

381   combined contribute to positive O_3 trends of 1.2±0.2 and 2.4±0.3 ppb/decade

382   in WUS and EUS, respectively. If the O_3 increase is attributed to NMVOCs

383   emissions, the combined natural source contribution is even larger (1.4±0.2 in

384   WUS and 2.5±0.2 ppb/decade in EUS) (Figs. 8f and 8h). O_3 produced by CH_4

385   increases at rates of 1.3±0.1 and 2.1±0.1 ppb/decade in WUS and EUS,

386   respectively, due to the weakened NO_x titration. Increases in aviation and

387   shipping emissions together explain the 1.2±0.1 and 1.5±0.1 ppb/decade of O_3

388   trends in WUS and EUS, respectively (Figs. 6e and 6g). Long-range transport

389   of O_3 produced from Asian NO_x emissions enhances the wintertime O_3

390   increasing trends by 0.9±0.1 and 1.2±0.1 ppb/decade in WUS and EUS,

391   respectively, which are equally contributed by sources from East Asia, South

392   Asia, and Southeast Asia (Figs. 8e and 8g).

393   **3.4. Impact of variations in large-scale circulations on ozone trends**

394   Many studies have reported that O_3 spatial distribution is strongly

395   modulated by changes in large-scale circulations (e.g., Shen and Mickley, 2017;

396   Yang et al., 2014, 2022). Based on our MET experiments with anthropogenic

397   emissions kept unchanged, the changes in large-scale circulations show a

398   weak influence on the U.S. O_3 trends in summer (Fig. 9a) but cause a significant

399   O_3 rise in the central U.S. in winter (Fig. 9b). Averaged over the U.S., the near-

400   surface O_3 mixing ratio in winter increases at the rate of 0.7±0.3 ppb/decade

401   during 1995–2019 in MET experiments. It suggests that the variation in large-

402   scale circulations is responsible for 15% of the increasing trend in wintertime

403   O_3 mixing ratio by 4.7±0.3 ppb/decade in the U.S. during 1995–2019 simulated

404   in BASE experiment.

405   The changes in atmospheric circulation pattern support the above finding.

406   Compared to 1995–1999, anomalous northerly winds locate over high latitudes

407   of North America in 2015–2019 (Fig. 9c), strengthening the prevailing northerly

408   winds in winter. In addition, an anomalous subsidence occurs over the central

409   U.S. in 2015–2019, compared to 1995–1999 (Fig. 9d). The anomalous

410   subsidence transport O_3 from high altitudes and even stratosphere to the

411   surface and the strengthened winds transport O_3 from remote regions (e.g., O_3

412   produced by Asian NO_x emission) to the central U.S., both contributing to

413   0.2±0.1 ppb/decade of the O_3 increase over the U.S. (Fig. 10). The finding is

414   consistent with Lin et al. (2015) that variations in the circulation facilitate O_3

415   transport from upper altitudes to the surface, as well as foreign contributions

416   from Asia. The anomalous atmospheric circulation is likely linked to the location

417   of the midlatitude jet stream, which is influenced by ENSO cycle.

418

419   **4. Conclusions and discussions**

420   Using a global chemistry–climate model equipped with an O_3 source

421   tagging technique, we examine the long-term trends and source apportionment

422   of O_3 in the continental U.S. over 1995–2019 to various emission source

423   sectors and regions in this study. This model can capture the O_3 decreasing

424   trend over the EUS in summer and increasing trend over the WUS in winter

425   during this time period, but largely overestimates the decreasing trend over

426   WUS in summer and increasing trend over EUS in winter.

427   In summer, our simulation results show that the decline in surface O_3 is

428   dominated by the rapid reductions in NO_x emissions from energy and surface

429   transportation sectors, contributing to O_3 decreases at a rate of –2.0 and –1.6

430   ppb/decade in WUS and –3.2 and –1.7 ppb/decade in EUS, respectively. As

431   the anthropogenic NO_x decreases, the more NO_x-sensitive condition leads to a

432   positive O_3 trend of 0.7 and 1.7 ppb/decade in WUS and EUS, respectively,

433   contributed by the NO_x emissions from soil. Due to the reductions in NO_x

434   emissions, the O_3 production efficiency by reactive carbon species also

435   decreased, leading to the decreasing contributions to O_3 from reactive carbon

436   species in summer during 1995–2019. Even though biogenic NMVOCs

437   emissions and CH_4 mixing ratio were fixed during simulations, their

438   contributions also decreased related to the weakened O_3 production efficiency

439   by these precursors. Source region tagging suggests that the domestic

440   emission reductions are primarily responsible for the decreasing trend in

441   summertime near-surface O_3 mixing ratios in the U.S. during 1995–2019.

442   The mechanisms of wintertime O_3 increases over the U.S. are more

443   complicated. First, the domestic emission control weakens the NO_x titration,

444   resulting in considerable increases in O_3 originating from natural sources,

445   including O_3 from stratospheric intrusion, lightning, soil and biogenic emissions.

446   The natural sources combined contribute a positive O_3 trend of more than 1 and

447   2 ppb/decade in WUS and EUS, respectively. Second, increases in aviation and

448   shipping emissions together explain the 1.2 and 1.5 ppb/decade of O_3 trends in

449   WUS and EUS, respectively. Third, long-range transport of O_3 produced from

450   Asian NO_x emissions enhances the wintertime O_3 increasing trends by 0.9 and

451   1.2 ppb/decade in WUS and EUS, respectively. Fourth, the variation of

452   horizontal and vertical transport O_3 associated with the changes in large-scale

453   circulation contributes to the near-surface O_3 increases over the U.S. by 15%

454   in winter during 1995–2019.

455   Compared to observations, the decreasing trend of O_3 mixing ratios over

456   WUS in summer and increasing trend over EUS in winter are overestimated in

457   the CAM4-chem model. Because most O_3 monitors are located in urban areas

458   and these areas generate strong O_3 during the day and have strong oxidation

459   titration at night, the daily and grid averaged O_3 mixing ratios output by the

460   model could be inconsistent with the urban observations. The overestimate of

461   O_3 trend in the EUS might be related to a potential biased model representation

462   of vertical mixing in winter. Large uncertainties existing in the emissions also

463   result in the biases in the O_3 simulation. Lin et al. (2017) found that the

464   contribution from increasing Asian emissions offset that from the U.S. emission

465   reductions, resulting in a weak O_3 trend in WUS. In this study, the Asian NO_x

466   emissions only contribute to 0.6 ppb/decade of the total positive trend in WUS

467   in summer, much lower than the 3.7 ppb/decade decrease attributable to the

468   domestic emission reductions, suggesting that the Asian contribution to the O_3

469   trends in WUS is possibly underestimated in this study. We also found that the

470   model did not capture the significant increase in summertime O_3 levels in China

471   in recent years, which could explain the low contribution from Asian sources.

472   Additionally, international shipping can have a disproportionately high influence

473   on tropospheric O_3 due to the dispersed nature of NO_x emissions (Butler et al.,

474   2020; Kasibhatla et al., 2000; von Glasow et al., 2003), together with the

475   weakened NO_x titration, resulting in the overestimation of O_3 trends. The fixed

476   CH_4 mixing ratio during simulations also biased the modeled O_3 trends, which

477   deserves further investigation with the varying CH_4 levels in future studies. The

478   coarse model resolution also contributed to the biases. The overestimate of O_3

479   trend over EUS in winter, likely related to the bias in NO_x titration, implies the

480   overestimate of source contributions to the trends in magnitude.

481   Compared with Butler et al. (2018), the simulation in this study shares

482   similar source sector contributions to the zonal average of O_3 mixing ratios at

483   the surface and 400 hPa in 2010 (Figs. S7 and S8 in this study and Figs. 5 and

484   6 in Butler et al. (2018)). The contributions from the stratosphere and lightning

485 NO$_x$ are relatively higher in this study than Butler et al. (2018). This may be

486 related to the different anthropogenic emission inventories used, causing

487 different O$_3$ production/loss efficiencies by natural precursors. When comparing

488 the contributions from different source regions to surface O$_3$ mixing ratios in

489 North America, NO$_x$ emissions from East Asia, South Asia, North America, and

490 Europe contributed 2.2, 1.1, 8.3, and 0.7 ppb of the surface O$_3$ in North America,

491 respectively (Fig. S9) in this study, which are also similar to those from Fig. 4 in

492 Butler et al. (2020). Both studies show the contributions of anthropogenic

493 NMVOCs to surface O$_3$ mixing ratios in North America are less than 10 ppb.

494

495

Author contributions. YY designed the research; PL and SL performed simulations; PL analyzed the data. All authors including HW, KL, PW, BL, and HL discussed the results and wrote the paper.

Code and data availability. The CESM is maintained by NCAR and is provided freely to the community. The ozone tagging code has been described by Butler et al. (2018). The MERRA-2 reanalysis data are from NASA GESDISC data (https://goldsmr5.gesdisc.eosdis.nasa.gov/data/MERRA2/M2I6NVANA.5.12.4/, last access: 1 August 2022). The surface O_3 measurements in U.S. are obtained from the U.S. Environmental Protection Agency (https://aqs.epa.gov/aqsweb/airdata/download_files.html#Daily, last access: 1 August 2022). The modeling results are made available at https://doi.org/10.5281/zenodo.6891316 (last access: 1 August 2022).

Competing interests. The authors declare that they have no conflict of interest.

References

Atkinson, R.: Atmospheric chemistry of VOCs and NO_x, Atmos. Environ., 34, 2063-2101, https://doi.org/10.1016/S1352-2310(99)00460-4, 2000.

Bates, K. H. and Jacob, D. J.: An Expanded Definition of the Odd Oxygen Family for Tropospheric Ozone Budgets: Implications for Ozone Lifetime and Stratospheric Influence, Geophys. Res. Lett., 47, e2019GL084486, https://doi.org/10.1029/2019gl084486, 2020.

Butler, T., Lupascu, A., and Nalam, A.: Attribution of ground-level ozone to anthropogenic and natural sources of nitrogen oxides and reactive carbon in a global chemical transport model, Atmos. Chem. Phys., 20, 10707-10731, https://doi.org/10.5194/acp-20-10707-2020, 2020.

Butler, T., Lupascu, A., Coates, J., and Zhu, S.: TOAST 1.0: Tropospheric Ozone Attribution of Sources with Tagging for CESM 1.2.2, Geosci. Model Dev, 11, 2825–2840, https://doi.org/10.5194/gmd-11-2825-2018, 2018.

Castellanos, P. and Boersma, K. F.: Reductions in nitrogen oxides over Europe driven by environmental policy and economic recession, Sci. Rep., 2, 265, https://doi.org/10.1038/srep00265, 2012.

Cheng, J., Tong, D., Liu, Y., Yu, S., Yan, L., Zheng, B., Geng, G., He, K., and Zhang, Q.: Comparison of current and future $PM_{2.5}$ air quality in China under CMIP6 and DPEC emission scenarios, Geophys. Res. Lett., 48, e2021GL093197, https://doi.org/10.1029/2021GL093197, 2021.

Collet, S., Kidokoro, T., Karamchandani, P., Jung, J., and Shah, T.: Future year ozone source attribution modeling study using CMAQ-ISAM, J. Air Waste Manag. Assoc., 68, 1239-1247, https://doi.org/10.1080/10962247.2018.1496954, 2018.

Cooper, O. R., Gao, R.-S., Tarasick, D., Leblanc, T., and Sweeney, C.: Long-term ozone trends at rural ozone monitoring sites across the United States, 1990-2010, J. Geophys. Res. Atmos., 117, D22307, https://doi.org/10.1029/2012JD018261, 2012.

Cooper, O. R., Schultz, M. G., Schröder, S., Chang, K.-L., Gaudel, A., Gerardo, Benítez, C., Cuevas, E., Fröhlich, M., Galbally, I. E., Kubistin, D., Lu, X., Audra, McClure-Begley, A., Molloy, S., Nédélec, P., O'Brien, J., Oltmans, S. J., Irina, Petropavlovskikh, I., Ries, L., Senik, I., Sjöberg, K., Solberg, S., Spain, T. G.,

566 Spangl, W., Steinbacher, M., Tarasick, D., Thouret, V., and Xu, X.: Multi-decadal
567 surface ozone trends at globally distributed remote locations, Elem. Sci. Anth.,
568 8, 23, https://doi.org/10.1525/elementa.420, 2020.
569
570 Clappier, A., Belis, C. A., Pernigotti, D., and Thunis, P.: Source apportionment
571 and sensitivity analysis: two methodologies with two different purposes, Geosci.
572 Model Dev., 10, 4245–4256, https://doi.org/10.5194/gmd-10-4245-2017, 2017.
573
574 Duncan, B. N., Lamsal, L. N., Thompson, A. M., Yoshida, Y., Lu, Z., Streets, D.
575 G., Hurwitz, M. M., and Pickering, K. E.: A space-based, high-resolution view of
576 notable changes in urban NO_x pollution around the world (2005–2014), J J.
577 Geophys. Res. Atmos., 21, 976-996, https://doi.org/10.1002/2015JD024121,
578 2016.
579
580 Dunker, A. M., Yarwood, G., Ortmann, J. P., and Wilson, G. M.: Comparison of
581 Source Apportionment and Source Sensitivity of Ozone in a Three-Dimensional
582 Air Quality Model, Environ. Sci. Technol., 36, 2953–2964,
583 https://doi.org/10.1021/es011418f, 2002.
584
585 Emmons, L. K., Hess, P. G., Lamarque, J.-F., and Pfister, G. G.: Tagged ozone
586 mechanism for MOZART-4, CAM-chem and other chemical transport models,
587 Geosci. Model Dev., 5, 1531–1542, https://doi.org/10.5194/gmd-5-1531-2012,
588 2012.
589
590 Emmons, L. K., Walters, S., Hess, P. G., Lamarque, J.-F., Pfister, G. G., Fillmore,
591 D., Granier, C., Guenther, A., Kinnison, D., Laepple, T., Orlando, J., Tie, X.,
592 Tyndall, G., Wiedinmyer, C., Baughcum, S. L., and Kloster, S.: Description and
593 evaluation of the Model for Ozone and Related chemical Tracers, version 4
594 (MOZART-4), Geosci. Model Dev., 3, 43–67, https://doi.org/10.5194/gmd-3-43-
595 2010, 2010.
596
597 Eyring, V., Köhler, H. W., van Aardenne, J., and Lauer, A.: Emissions from
598 international shipping: 1. The last 50 years, J. Geophys. Res., 110, D17305,
599 https://doi.org/10.1029/2004JD005619, 2005.
600
601 Fan, T., Liu, X., Ma, P.-L., Zhang, Q., Li, Z., Jiang, Y., Zhang, F., Zhao, C., Yang,
602 X., Wu, F., and Wang, Y.: Emission or atmospheric processes? An attempt to
603 attribute the source of large bias of aerosols in eastern China simulated by
604 global climate models, Atmos. Chem. Phys., 18, 1395–1417,
605 https://doi.org/10.5194/acp-18-1395-2018, 2018.
606
607 Fiore, A. M., West, J. J., Horowitz, L. W., Naik, V., and Schwarzkopf, M. D.:

Characterizing the tropospheric ozone response to methane emission controls and the benefits to climate and air quality, J. Geophys. Res., 113, D08307, https://doi.org/10.1029/2007JD009162, 2008.

Fiore, A. M., Dentener, F. J., Wild, O., Cuvelier, C., Schultz, M. G., Hess, P., Textor, C., Schulz, M., Doherty, R. M., Horowitz, L. W., MacKenzie, I. A., Sanderson, M. G., Shindell, D. T., Stevenson, D. S., Szopa, S., van Dingenen, R., Zeng, G., Atherton, C., Bergmann, D., Bey, I., Carmichael, G., Collins, W. J., Duncan, B. N., Faluvegi, G., Folberth, G., Gauss, M., Gong, S., Hauglustaine, D., Holloway, T., Isaksen, I. S. A., Jacob, D. J., Jonson, J. E., Kaminski, J. W., Keating, T. J., Lupu, A., Marmer, E., Montanaro, V., Park, R. J., Pitari, G., Pringle, K. J., Pyle, J. A., Schroeder, S., Vivanco, M. G., Wind, P., Wojcik, G., Wu, S., and Zuber, A.: Multimodel estimates of intercontinental source-receptor relationships for ozone pollution, J. Geophys. Res., 114, D04301 , https://doi.org/10.1029/2008JD010816, 2009.

Fleming, Z. L., Doherty, R. M., Schneidemesser, E. V., Malley, C. S., Cooper, O. R., Pinto, J. P., Colette, A., Xu, X., Simpson, D., Schultz, M. G., Lefohn, A. S., Hamad, S., Moolla, R., Solberg, S., and Feng, Z.: Tropospheric Ozone Assessment Report: Present-day ozone distribution and trends relevant to human health, Elem. Sci. Anth., 6, 12, https://doi.org/10.1525/elementa.273, 2018.

Gao, J., Zhu, B., Xiao, H., Kang, H., Hou, X., and Shao, P.: A case study of surface ozone source apportionment during a high concentration episode, under frequent shifting wind conditions over the Yangtze River Delta, China, Sci. Total Environ., 544, 853-863, https://doi.org/10.1016/j.scitotenv.2015.12.039, 2016.

Gao, Y., Fu, J. S., Drake, J. B., Lamarque, J. F., and Liu, Y.: The impact of emission and climate change on ozone in the United States under representative concentration pathways (RCPs), Atmos. Chem. Phys., 13, 9607-9621, https://doi.org/10.5194/acp-13-9607-2013, 2013.

Gaudel, A., Cooper, O. R. , Chang, K. L., Bourgeois, I., Ziemke, J. R., Strode, S. A., Oman, L. D., Sellitto, P., Nédélec, P., Bolt, R., Thouret, V. and Granier,C.: Aircraft observations since the 1990s reveal increases of tropospheric ozone at multiple locations across the Northern Hemisphere, Sci. Adv., 6, eaba8272, https://doi.org/10.1126/sciadv.aba8272, 2020.

Gelaro, R., McCarty, W., Suárez, M. J., Todling, R., Molod, A., Takacs, L., Randles, C. A., Darmenov, A., Bosilovich, M. G., Re- ichle, R., Wargan, K., Coy,

650 L., Cullather, R., Draper, C., Akella, S., Buchard, V., Conaty, A., da Silva, A. M.,
651 Gu, W., Kim, G., Koster, R., Lucchesi, R., Merkova, D., Nielsen, J. E., Partyka,
652 G., Pawson, S., Putman, W., Rienecker, M., Schubert, S. D., Sienkiewicz, M.,
653 and Zhao, B.: The Modern-Era Retrospective Analysis for Research and
654 Applications, Version 2 (MERRA-2), J. Climate, 30, 5419–5454,
655 https://doi.org/10.1175/JCLI-D-16- 0758.1, 2017.

657 Grewe, V., Tsati, E., Mertens, M., Frömming, C., and Jöckel, P.: Contribution of
658 emissions to concentrations: the TAGGING 1.0 submodel based on the
659 Modular Earth Submodel System (MESSy 2.52), Geosci. Model Dev., 10,
660 2615–2633, https://doi.org/10.5194/gmd-10-2615-2017, 2017.

662 Haagen-Smit, A. J.: Chemistry and Physiology of Los Angeles Smog, Ind. Eng.
663 Chem., 44, 1342-1346, https://doi.org/10.1021/ie50510a045, 1952.

665 Hodnebrog, Ø., Berntsen, T. K., Dessens, O., Gauss, M., Grewe, V., Isaksen, I.
666 S. A., Koffi, B., Myhre, G., Olivié, D., Prather, M. J., Pyle, J. A., Stordal, F., Szopa,
667 S., Tang, Q., van Velthoven, P., Williams, J. E., and Ødemark, K.: Future impact
668 of non-land based traffic emissions on atmospheric ozone and OH – an
669 optimistic scenario and a possible mitigation strategy, Atmos. Chem. Phys., 11,
670 11293–11317, https://doi.org/10.5194/acp-11-11293-2011, 2011.

672 Hoesly, R. M., Smith, S. J., Feng, L., Klimont, Z., Janssens-Maenhout, G.,
673 Pitkanen, T., Seibert, J. J., Vu, L., Andres, R. J., Bolt, R. M., Bond, T. C.,
674 Dawidowski, L., Kholod, N., Kurokawa, J.-I., Li, M., Liu, L., Lu, Z., Moura, M. C.
675 P., O'Rourke, P. R., and Zhang, Q.: Historical (1750–2014) anthropogenic
676 emissions of reactive gases and aerosols from the Community Emissions Data
677 System (CEDS), Geosci. Model Dev., 11, 369–408,
678 https://doi.org/10.5194/gmd-11-369-2018, 2018.

680 Han, H., Liu, J., Yuan, H., Zhuang, B., Zhu, Y., Wu, Y., Yan, Y., and Ding, A.:
681 Characteristics of intercontinental transport of tropospheric ozone from Africa
682 to Asia, Atmos. Chem. Phys., 18, 4251–4276, https://doi.org/10.5194/acp-18-
683 4251-2018, 2018.

685 Hoor, P., Borken-Kleefeld, J., Caro, D., Dessens, O., Endresen, Ø., Gauss, M.,
686 Grewe, V., Hauglustaine, D. A., Isaksen, I. S. A., Jöckel, P., Lelieveld, J., Myhre,
687 G., Meijer, E. W., Olivié, D., Prather, M. J., Poberaj, C. S., Shine, K. P., Staehelin,
688 J., Tang, Q., Aardenne, J. v., Velthoven, P. F. J. v., and Sausen, R.: The impact
689 of traffic emissions on atmospheric ozone and OH: results from QUANTIFY,
690 Atmos. Chem. Phys., 9, 3113-3116, https://doi.org/10.5194/acp-9-3113-2009,
691 2009.

692

693 Jaffe, D. A., Cooper, O. R., Fiore, A. M., Henderson, B. H., Tonnesen, G. S.,
694 Russell, A. G., Henze, D. K., Langford, A. O., Lin, M., and Moore, T.: Scientific
695 assessment of background ozone over the U.S.: Implications for air quality
696 management, Elem. Sci. Anth, 6, 56, https://doi.org/
697 https://doi.org/10.1525/elementa.309, 2018.

698

699 Johnson, C., Collins, W., Stevenson, D., and Derwent, R.: Relative roles of
700 climate and emissions changes on future tropospheric oxidant concentrations,
701 J. Geophys. Res., 104, 18631–18645, https://doi.org/10.1029/1999JD900204,
702 1999.

703

704 Kasibhatla, P., Levy, H., Moxim, W. J., Pandis, S. N., Corbett, J. J., Peterson,
705 M. C., Honrath, R. E., Frost, G. J., Knapp, K., Parrish, D. D., and Ryerson, T.
706 B.: Do emissions from ships have a significant impact on concentrations of
707 nitrogen oxides in the marine boundary layer?, Geophys. Res. Lett., 27, 2229–
708 2232, https://doi.org/10.1029/2000gl011387, 2000.

709

710 Koo, B., Wilson, G. M., Morris, R., Dunker, A. M., and Yarwood, G.: Comparison
711 of Source Apportionment and Sensitivity Analysis in a Particulate Matter Air
712 Quality Model, Environ. Sci. Technol., 43, 6669–6675,
713 https://doi.org/10.1021/es9008129, 2009.

714

715 Kwok, R. H. F., Baker, K. R., Napelenok, S. L., and Tonnesen, G. S.:
716 Photochemical grid model implementation and application of VOC, NO_x, and
717 O_3 source apportionment, Geosci. Model Dev., 8, 99–114,
718 https://doi.org/10.5194/gmd-8-99-2015, 2015.

719

720 Lamarque, J.-F., Emmons, L. K., Hess, P. G., Kinnison, D. E., Tilmes, S., Vitt,
721 F., Heald, C. L., Holland, E. A., Lauritzen, P. H., Neu, J., Orlando, J. J., Rasch,
722 P. J., and Tyndall, G. K.: CAM-chem: description and evaluation of interactive
723 atmospheric chemistry in the Community Earth System Model, Geosci. Model
724 Dev., 5, 369–411, https://doi.org/10.5194/gmd-5-369-2012, 2012.

725

726 Lin, M., Fiore, A. M., Horowitz, L. W., Langford, A. O., Oltmans, S. J., Tarasick,
727 D., and Rieder, H. E.: Climate variability modulates western U.S. ozone air
728 quality in spring via deep stratospheric intrusions, Nat. Commun., 6, 7105,
729 https://doi.org/10.1038/ncomms8105, 2015.

730

731 Lin, M., Horowitz, L. W., Payton, R., Fiore, A. M., and Tonnesen, G. S.: US
732 surface ozone trends and extremes from 1980 to 2014: quantifying the roles of
733 rising Asian emissions, domestic controls, wildfires, and climate, Atmos. Chem.

734 Phys., 17, 2943–2970, https://doi.org/10.5194/acp-17-2943-2017, 2017.
735

736 Lupaşcu, A. and Butler, T.: Source attribution of European surface O_3 using a
737 tagged O_3 mechanism, Atmos. Chem. Phys., 19, 14535–14558,
738 https://doi.org/10.5194/acp-19-14535-2019, 2019.
739

740 Mertens, M., Kerkweg, A., Grewe, V., Jöckel, P., and Sausen, R.: Attributing
741 ozone and its precursors to land transport emissions in Europe and Germany,
742 Atmos. Chem. Phys., 20, 7843–7873, https://doi.org/10.5194/acp-20-7843-
743 2020, 2020.
744

745 McDuffie, E. E., Smith, S. J., O'Rourke, P., Tibrewal, K., Venkataraman, C.,
746 Marais, E. A., Zheng, B., Crippa, M., Brauer, M., and Martin, R. V.: A global
747 anthropogenic emission inventory of atmospheric pollutants from sector- and
748 fuel-specific sources (1970–2017): an application of the Community Emissions
749 Data System (CEDS), Earth Syst. Sci. Data, 12, 3413–3442,
750 https://doi.org/10.5194/essd-12-3413-2020, 2020.
751

752 Müller-Casseres, E., Edelenbosch, O. Y., Szklo, A., Schaeffer, R., and van
753 Vuuren, D. P.: Global futures of trade impacting the challenge to decarbonize
754 the international shipping sector, Energy, 237, 121547,
755 https://doi.org/10.1016/j.energy.2021.121547, 2021
756

757 Myhre, G., D. Shindell, F.-M. Bréon, W. Collins, J. Fuglestvedt, J. Huang, D.
758 Koch, J.-F. Lamarque, D. Lee, B. Mendoza, T. Nakajima, A. Robock, G.
759 Stephens, T. Takemura and H. Zhang, 2013: Anthropogenic and Natural
760 Radiative Forcing. In: Climate Change 2013: The Physical Science Basis.
761 Contribution of Working Group I to the Fifth Assessment Report of the
762 Intergovernmental Panel on Climate Change [Stocker, T.F., D. Qin, G.-K.
763 Plattner, M. Tignor, S.K. Allen, J. Boschung, A. Nauels, Y. Xia, V. Bex and P.M.
764 Midgley (eds.)]. Cambridge University Press, Cambridge, United Kingdom and
765 New York, NY, USA, 2013.
766

767 Neu, J. L. and Prather, M. J.: Toward a more physical representation of
768 precipitation scavenging in global chemistry models: cloud overlap and ice
769 physics and their impact on tropospheric ozone, Atmos. Chem. Phys. Discuss.,
770 11, 24413–24466, https://doi.org/10.5194/acpd-11-24413-2011, 2011
771

772 O'Neill, B. C., Tebaldi, C., van Vuuren, D. P., Eyring, V., Friedlingstein, P., Hurtt,
773 G., Knutti, R., Kriegler, E., Lamarque, J.-F., Lowe, J., Meehl, G. A., Moss, R.,
774 Riahi, K., and Sanderson, B. M.: The Scenario Model Intercomparison Project
775 (ScenarioMIP) for CMIP6, Geosci. Model Dev., 9, 3461-3482,

https://doi.org/10.5194/gmd-9-3461-2016, 2016.

Price, C., Penner, J., and Prather, M.: NO_x from lightning 1, Global distribution based on lightning physics, J. Geophys. Res., 102, 5929–5941, https://doi.org/10.1029/96JD03504, 1997.

Seinfeld, J. H. and Pandis, S. N.: Atmospheric Chemistry and Physics: From Air Pollution to Climate Change, J. Wiley, Hoboken, N.J., 2006.

Simon, H., Reff, A., Wells, B., Xing, J., and Frank, N.: Ozone trends across the United States over a period of decreasing NO_x and VOC emissions, Environ. Sci. Technol., 49, 186-195, https://doi.org/10.1021/es504514z, 2015.

Shen, L. and Mickley, L. J.: Effects of El Niño on summertime ozone air quality in the eastern United States, Geophys. Res. Lett., 44, 12543–12550, https://doi.org/10.1002/2017GL076150, 2017.

Stevenson, D. S., Dentener, F. J., Schultz, M. G., Ellingsen, K., van Noije, T. P. C., Wild, O., Zeng, G., Amann, M., Atherton, C. S., Bell, N., Bergmann, D. J., Bey, I., Butler, T., Cofala, J., Collins, W. J., Derwent, R. G., Doherty, R. M., Drevet, J., Eskes, H. J., Fiore, A. M., Gauss, M., Hauglustaine, D. A., Horowitz, L. W., Isaksen, I. S. A., Krol, M. C., Lamarque, J.-F., Lawrence, M. G., Montanaro, V., Müller, J.-F., Pitari, G., Prather, M. J., Pyle, J. A., Rast, S., Rodriguez, J. M., Sanderson, M. G., Savage, N. H., Shindell, D. T., Strahan, S. E., Sudo, K., and Szopa, S.: Multimodel ensemble simulations of present-day and near-future tropospheric ozone, J. Geophys. Res., 111, D08301. https://doi.org/10.1029/2005JD006338, 2006.

Sudo, K., and Akimoto, H.: Global source attribution of tropospheric ozone: Long-range transport from various source regions, J. Geophys. Res., 112, D12302, https://doi.org/10.1029/2006JD007992, 2007.

Szopa, S., Naik, V., Adhikary, B., Artaxo, P., Berntsen, T., Collins, W.D., Fuzzi, S., Gallardo, L., Kiendler-Scharr, A., Klimont, Z., Liao, H., Unger, N. and Zanis, P., 2021: Short-Lived Climate Forcers. In Climate Change 2021: The Physical Science Basis. Contribution of Working Group I to the Sixth Assessment Report of the Intergovernmental Panel on Climate Change [Masson-Delmotte, V., Zhai, P., Pirani, A., Connors, S.L., Péan, C., Berger, S., Caud, N., Chen, Y., Goldfarb, L., Gomis, M.I., Huang, M., Leitzell, K., Lonnoy, E., Matthews, J.B.R., Maycock, T.K., Waterfield, T., Yelekçi, O., Yu, R. and Zhou B. (eds.)]. Cambridge University Press, Cambridge, United Kingdom and New York, NY, USA, pp. 817–922, doi:10.1017/9781009157896.008, 2021.

818

819 Thor, R. N., Mertens, M., Matthes, S., Righi, M., Hendricks, J., Brinkop, S., Graf,
820 P., Grewe, V., Jöckel, P., and Smith, S.: An inconsistency in aviation emissions
821 between CMIP5 and CMIP6 and the implications for short-lived species and
822 their radiative forcing, Geosci. Model Dev., 16, 1459–1466,
823 https://doi.org/10.5194/gmd-16-1459-2023, 2023.

824

825 Thunis, P., Clappier, A., Tarrason, L., Cuvelier, C., Monteiro, A., Pisoni, E.,
826 Wesseling, J., Belis, C., Pirovano, G., Janssen, S., Guerreiro, C., and Peduzzi,
827 E.: Source apportionment to support air quality planning: Strengths and
828 weaknesses of existing approaches, Environ. Int., 130, 104825,
829 https://doi.org/10.1016/j.envint.2019.05.019, 2019.

830

831 Tilmes, S., Lamarque, J. F., Emmons, L. K., Kinnison, D. E.,Marsh, D., Garcia,
832 R. R., Smith, A. K., Neely, R. R., Conley, A., Vitt, F., V al Martin, M., Tanimoto,
833 H., Simpson, I., Blake, D. R., and Blake, N.: Representation of the Community
834 Earth System Model (CESM1) CAM4-chem within the Chemistry-Climate
835 Model Initiative (CCMI), Geosci. Model Dev., 9, 1853–1890,
836 https://doi.org/10.5194/gmd-9-1853-2016, 2016.

837

838 Tilmes, S., Lamarque, J. F., Emmons, L. K., Kinnison, D. E., Ma, P. L., Liu, X.,
839 Ghan, S., Bardeen, C., Arnold, S., Deeter, M., Vitt, F., Ryerson, T., Elkins, J. W.,
840 Moore, F., Spackman, J. R., and Val Martin, M.: Description and evaluation of
841 tropospheric chemistry and aerosols in the Community Earth System Model
842 (CESM1.2), Geosci. Model Dev., 8, 1395-1426, https://doi.org/10.5194/gmd-8-
843 1395-2015, 2015.

844

845 van Marle, M. J. E., Kloster, S., Magi, B. I., Marlon, J. R., Daniau, A.-L., Field,
846 R. D., Arneth, A., Forrest, M., Hantson, S., Kehrwald, N. M., Knorr, W., Lasslop,
847 G., Li, F., Mangeon, S., Yue, C., Kaiser, J. W., and van der Werf, G. R.: Historic
848 global biomass burning emissions for CMIP6 (BB4CMIP) based on merging
849 satellite observations with proxies and fire models (1750–2015), Geosci. Model
850 Dev., 10, 3329-3357, https://doi.org/10.5194/gmd-10-3329-2017, 2017.

851

852 von Glasow, R., Lawrence, M. G., Sander, R., and Crutzen, P. J.: Modeling the
853 chemical effects of ship exhaust in the cloud-free marine boundary layer, Atmos.
854 Chem. Phys., 3, 233–250, https://doi.org/10.5194/acp-3-233-2003, 2003.

855

856 Wang, H., Rasch, P. J., Easter, R. C., Singh, B., Zhang, R., Ma, P.-L., Qian, Y.,
857 Ghan, S. J., and Beagley, N.: Using an explicit emission tagging method in
858 global modeling of source-receptor relationships for black carbon in the Arctic:
859 Variations, sources, and transport pathways, J. Geophys. Res. Atmos., 119,

860   12888-12909, https://doi.org/10.1002/2014JD022297, 2014.

862   Wesely, M. L.: Parameterizations for surface resistance to gaseous dry
863   deposition in regional-scale numerical models, Atmos. Environ., 23, 1293–1304,
864   https://doi.org/10.1016/0004-6981(89)90153-4, 1989.

866   Xing, J., Pleim, J. E., Mathur, R., Pouliot, G., Hogrefe, C., Gan, C.-M., and Wei,
867   C.: Historical gaseous and primary aerosol emissions in the United States from
868   1990   to   2010,   Atmos.   Chem.   Phys.,   13,   7531–7549,
869   https://doi.org/10.5194/acp-13-7531-2013, 2013.

871   Yang, Y., Li, M., Wang, H., Li, H., Wang, P., Li, K., Gao, M., and Liao, H.: ENSO
872   modulation of summertime tropospheric ozone over China, Environ. Res. Lett.,
873   17, 034020, https://doi.org/10.1088/1748-9326/ac54cd, 2022.

875   Yang, Y., Liao, H., and Li, J.: Impacts of the East Asian summer monsoon on
876   interannual variations of summertime surface-layer ozone concentrations over
877   China, Atmos. Chem. Phys., 14, 6867–6879, https://doi.org/10.5194/acp-14-
878   6867-2014, 2014.

880   Yang, Y., Wang, H., Smith, S. J., Zhang, R., Lou, S., Yu, H., Li, C., and Rasch,
881   P. J.: Source apportionments of aerosols and their direct radiative forcing and
882   long-term trends over continental United States, Earth's Future, 6, 793–808,
883   https://doi.org/10.1029/2018EF000859, 2018.

885   Zhang, L., Jacob, D. J., Boersma, K. F., Jaffe, D. A., Olson, J. R., Bowman, K.
886   W., Worden, J. R., Thompson, A. M., Avery, M. A., Cohen, R. C., Dibb, J. E.,
887   Flock, F. M., Fuelberg, H. E., Huey, L. G., McMillan, W. W., Singh, H. B., and
888   Weinheimer, A. J.: Transpacific transport of ozone pollution and the effect of
889   recent Asian emission increases on air quality in North America: an integrated
890   analysis using satellite, aircraft, ozonesonde, and surface observations, Atmos.
891   Chem. Phys., 8, 6117–6136, https://doi.org/10.5194/acp-8-6117-2008, 2008.

893   Zhang, Y., Cooper, O. R., Gaudel, A., Nedelec, P., Ogino, S. Y., Thompson, A.
894   M., and West, J. J.: Tropospheric ozone change from 1980 to 2010 dominated
895   by equatorward redistribution of emissions, Nat. Geosci., 9, 875-879,
896   https://doi.org/10.1038/ngeo2827, 2016.

898   Zhang, Y., West, J. J., Emmons, L. K., Flemming, J., Jonson, J. E., Lund, M. T.,
899   Sekiya, T., Sudo, K., Gaudel, A., Chang, K. L., Nédélec, P., and Thouret, V.:
900   Contributions of World Regions to the Global Tropospheric Ozone Burden
901   Change From 1980 to 2010, Geophys. Res. Lett., 48, e2020GL089184,

902   https://doi.org/10.1029/2020GL089184, 2021.

903 **Table 1.** O_3 trends (ppb/decade) over eastern U.S. and western U.S. in winter
904 (December-January-February, DJF) and summer (June-July-August, JJA) from
905 observations and model simulations.
906

Season	Source	eastern U.S.	western U.S.
DJF	Observation	2.1 ± 0.29	2.2 ± 0.23
DJF	Model	6.1 ± 0.40	3.2 ± 0.28
JJA	Observation	-3.0±0.41	-0.5 ± 0.42
JJA	Model	-3.0±0.29	-2.3 ± 0.20

907
908
909

910

911
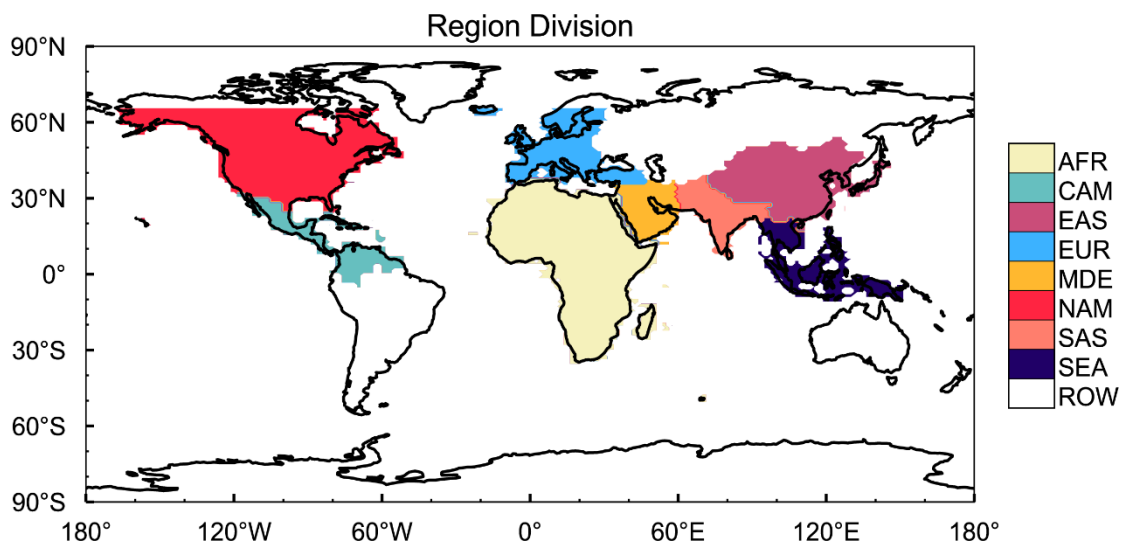
912 **Figure 1.** Source regions that are selected for O_3 source tagging in this study,

913 include Africa (AFR), Central America (CAM), East Asia (EAS), Europe (EUR),

914 Middle East (MDE), North America (NAM), South Asia (SAS), Southeast Asia

915 (SEA) and rest of the world (ROW).

916

(a) Summer 1995   R:0.33 NMB:24%

(b) Winter 1995   R:0.21 NMB:13%

(c) Summer 2019   R:0.45 NMB:28%

(d) Winter 2019   R:0.32 NMB:37%

ppb

0 5 10 15 20 25 30 35 40 45 50 55 60
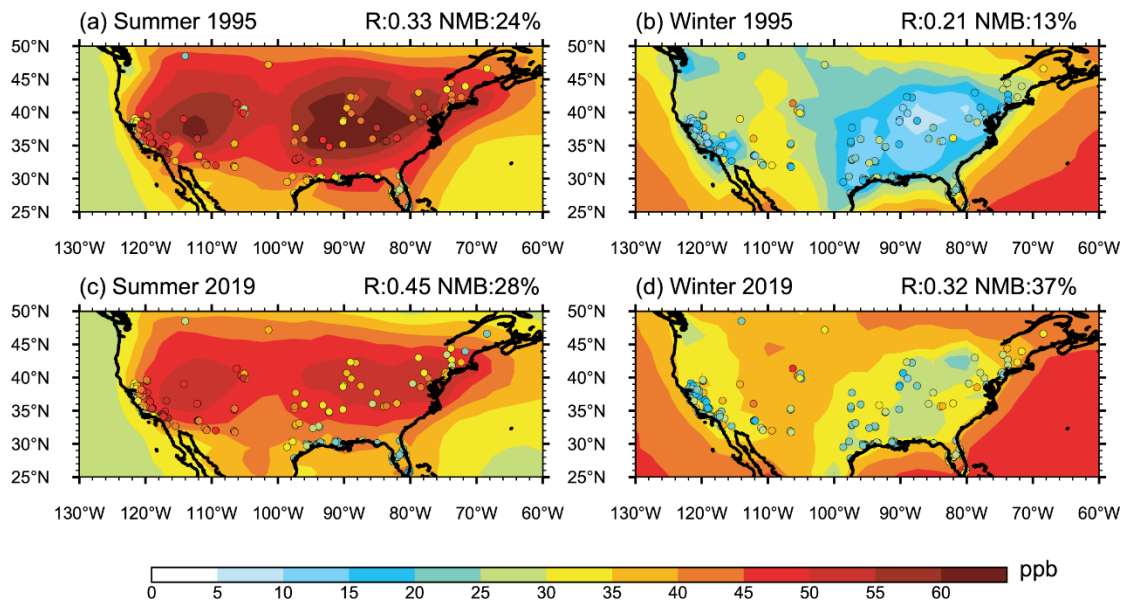
Figure 2. The simulated (contours) and observed (scatters) seasonal mean near-surface O3 mixing ratios over the United States in JJA (left) and DJF (right) and in 1995 (top) and 2019 (bottom). The correlation coefficient and normalized mean bias (NMB, $\sum$ (Model − Observation) / $\sum$ Observation $\times$ 100%) are shown on top right of each panel.
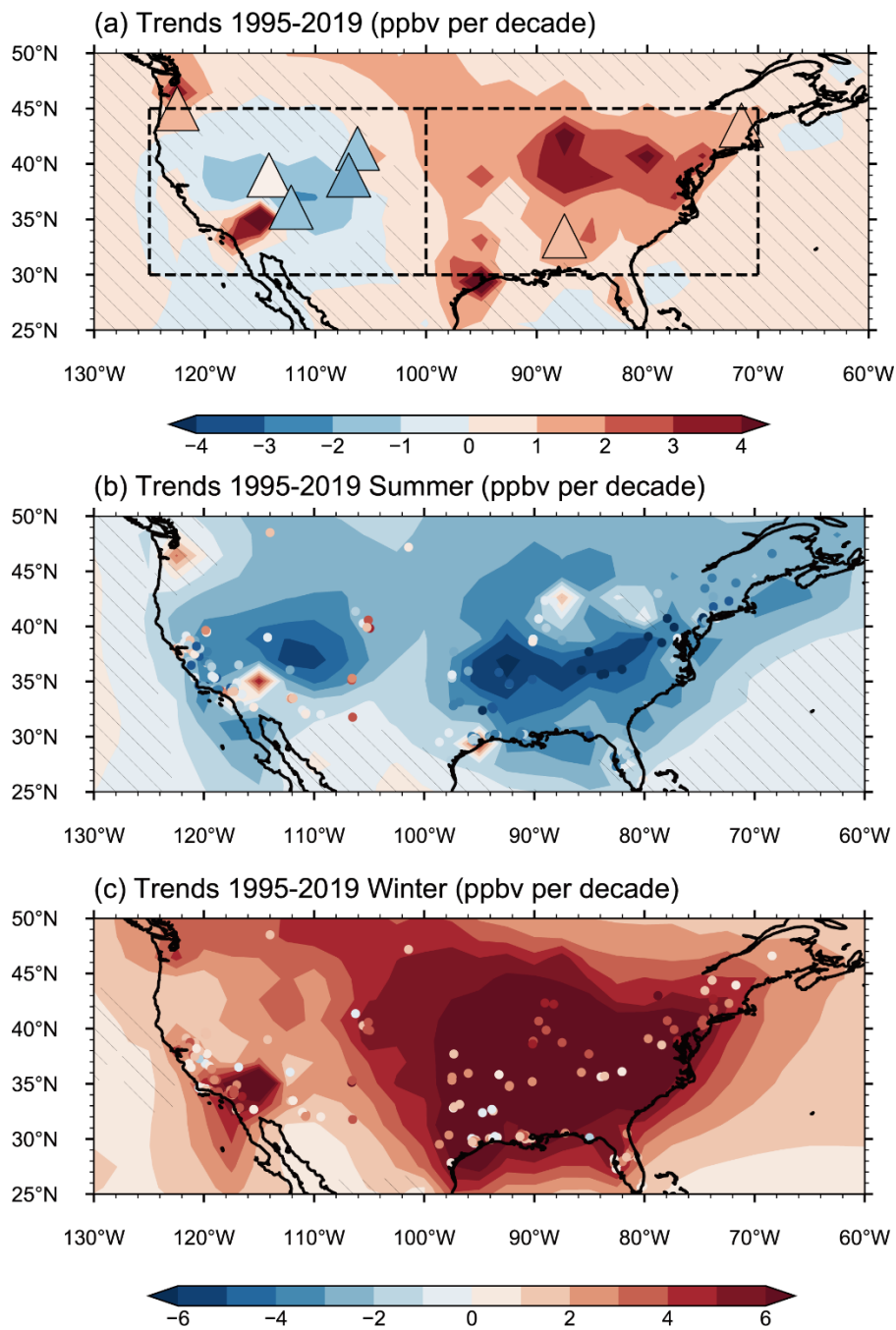
Figure 3. Linear trends (ppb/decade) of simulated (contours) and observed (color-filled markers) (a) annual, (b) JJA and (c) DJF mean near-surface O_3 mixing ratios during 1995–2019. Areas without hatches indicate statistical significance with 95% confidence. The boxes in (a) mark the western U.S. (WUS, 100–125°W, 30–45°N) and eastern U.S. (EUS, 70–100°W, 30–45°N), respectively. The observed annual O_3 mixing ratio trends in (a) are derived from IPCC AR6, based on Cooper et al. (2020) and Gaudel et al. (2020) over 1995–2017. The observed seasonal O_3 mixing ratio trends in (b) and (c) are calculated based on the U.S. EPA O_3 measurements over 1995–2019.
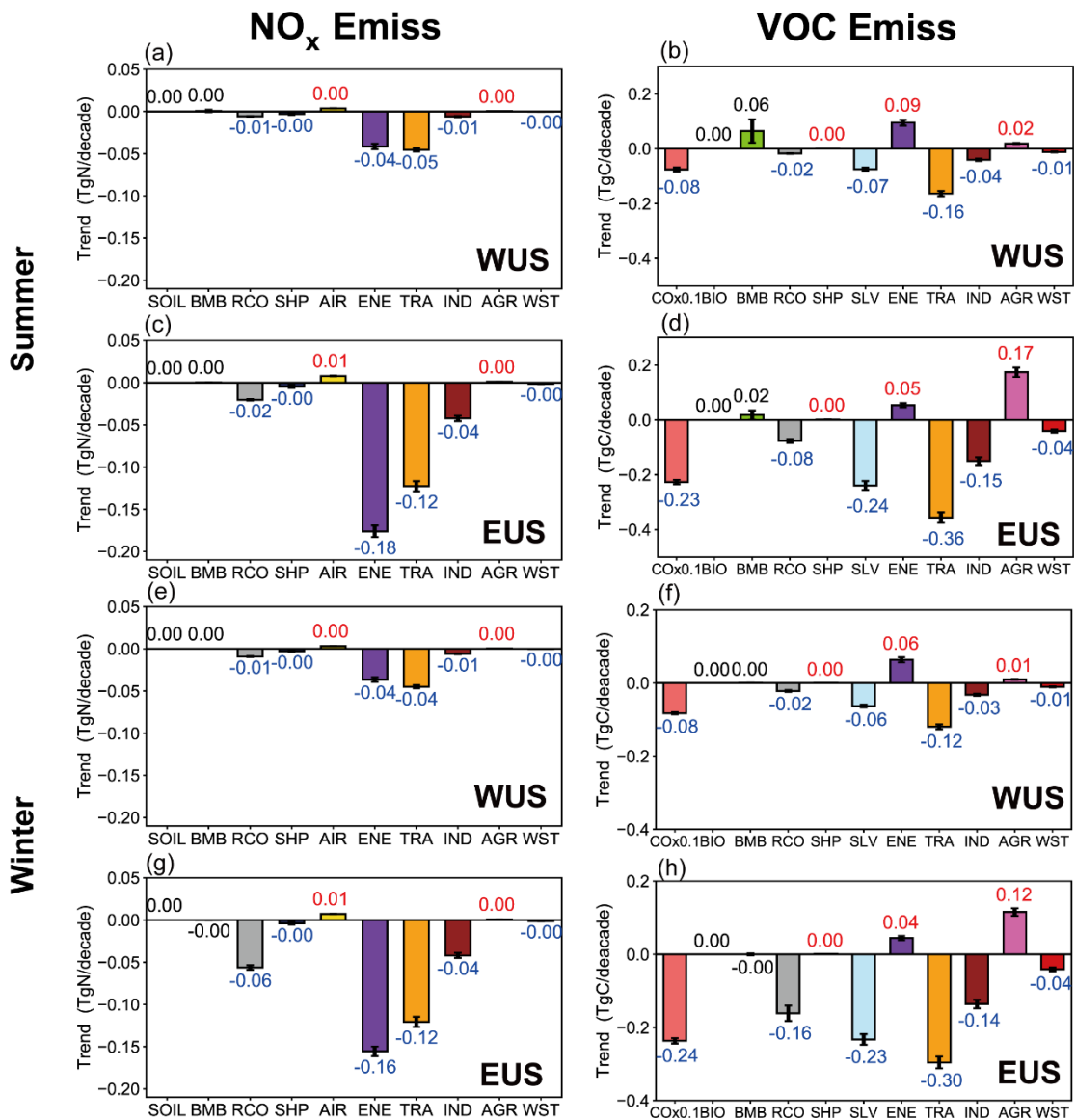
Figure 4. Linear trends of NOₓ and reactive carbon emissions from various sectors in summer and winter over WUS and EUS. The increasing and decreasing trends marked with red and blue values, respectively, indicate statistical significance with 95% confidence.
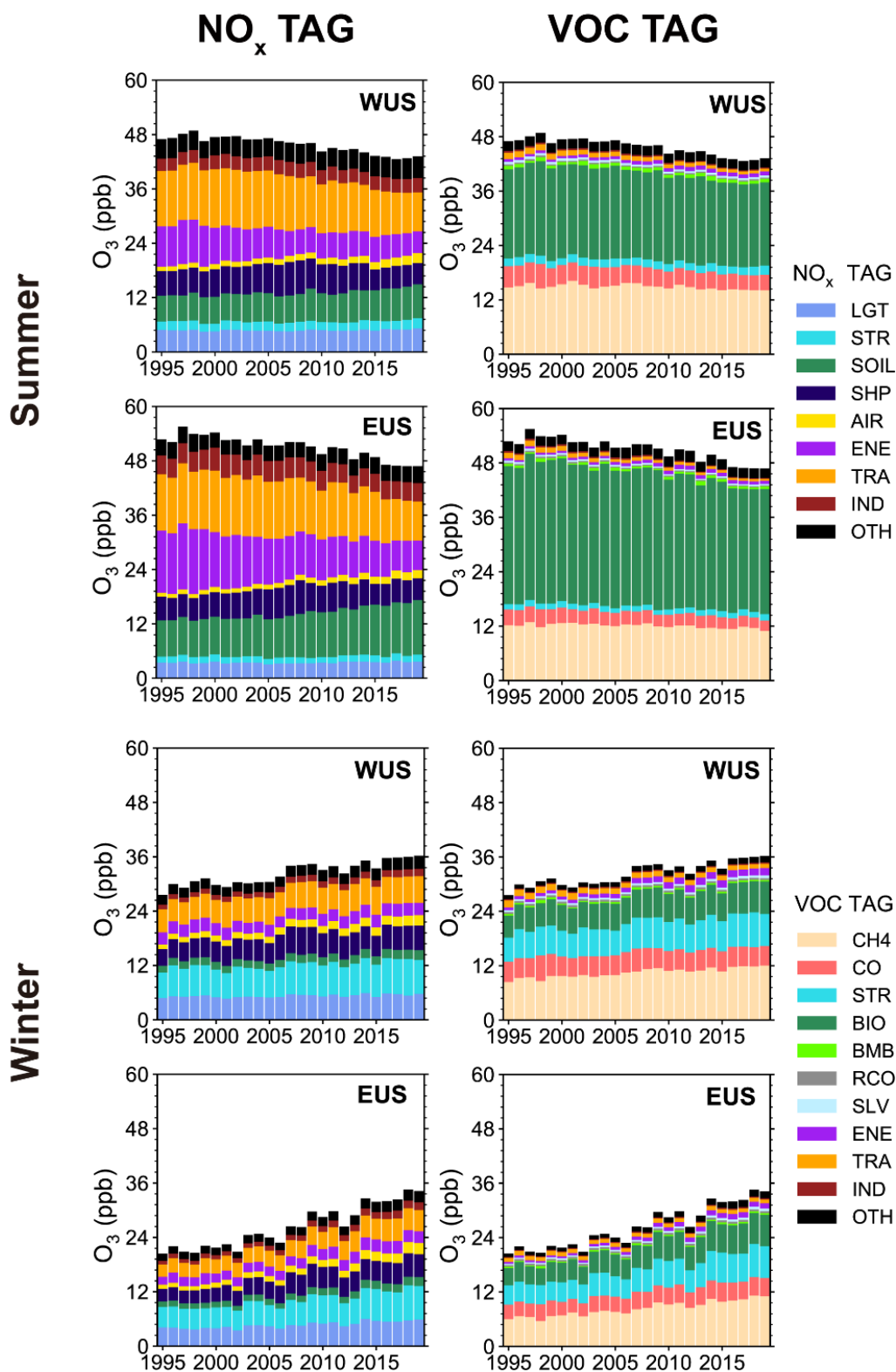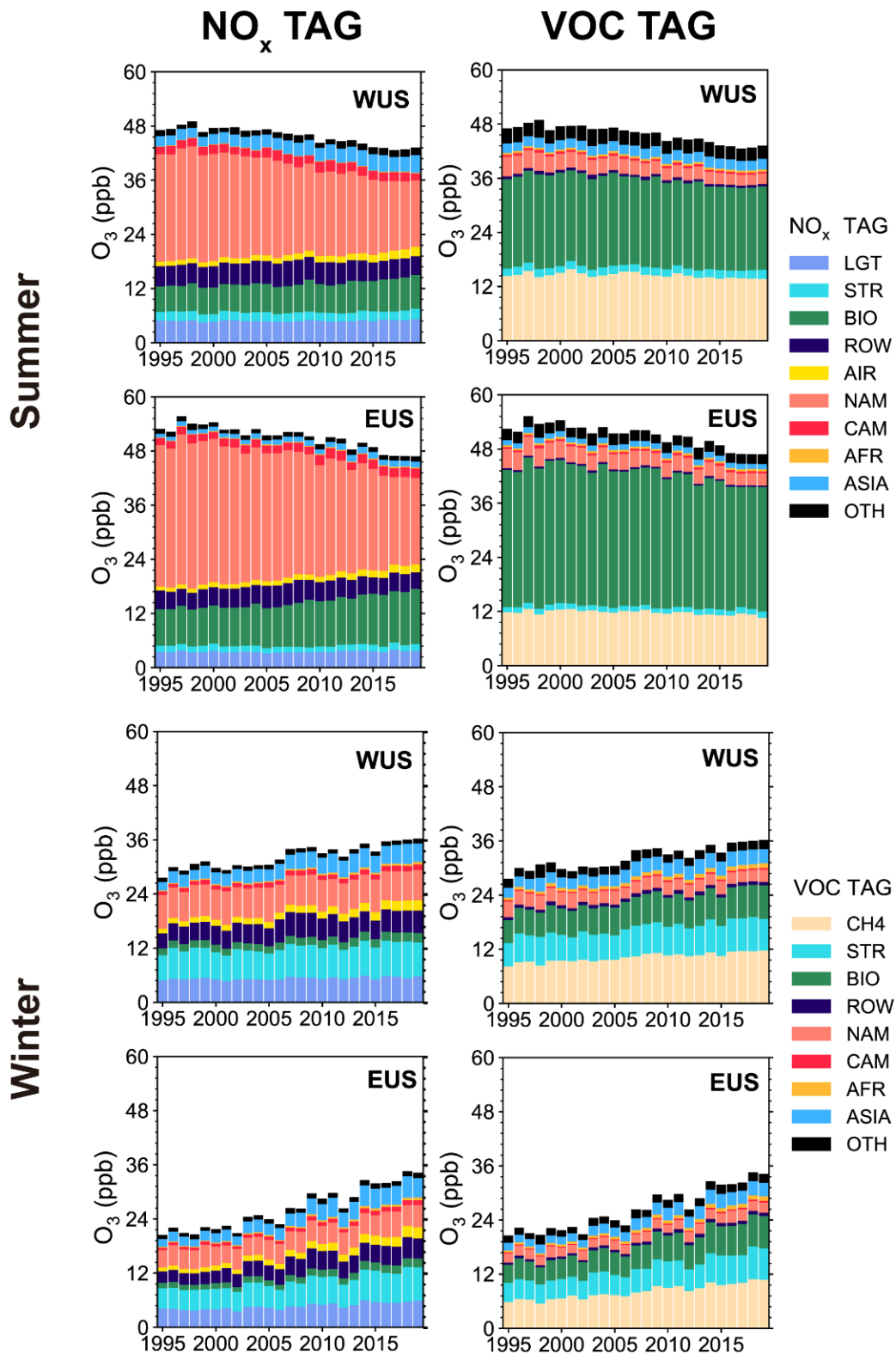
Figure 5. Time series of near-surface O_3 mixing ratios (ppb) averaged over WUS and EUS contributed by NO_x and reactive carbon emissions from different sectors in summer and winter during 1995–2019. Sources with small contributions are combined and shown as OTH.
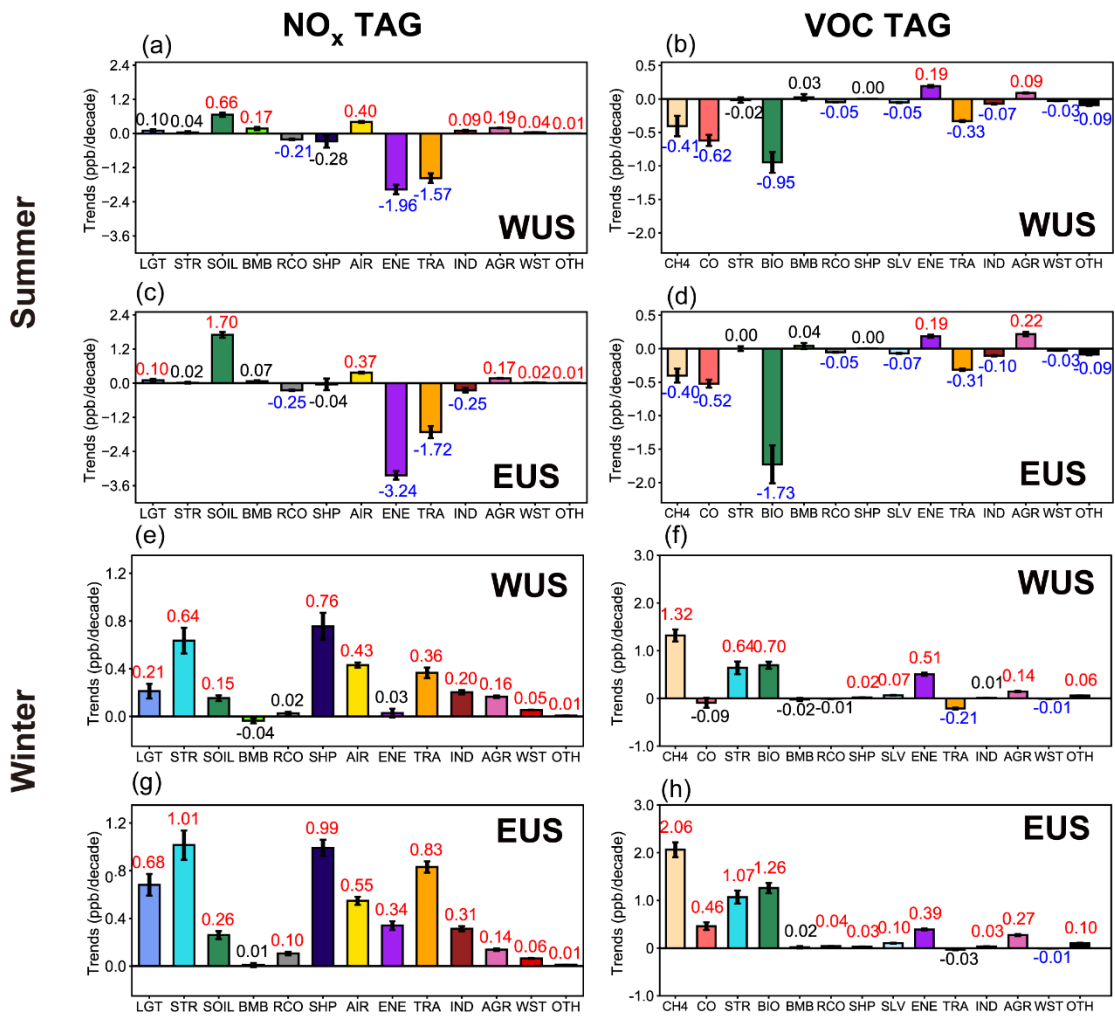
Figure 6. Linear trends (ppb/decade) of near-surface O_3 mixing ratios in summer and winter over WUS and EUS contributed by the NO_x (left) and reactive carbon (right) emissions from various sectors (color bars). The increasing and decreasing trends marked with red and blue color numbers, respectively, indicate statistical significance with 95% confidence. Other sources having small contributions are combined and shown as OTH.

Figure 7. Time series of near-surface O_3 mixing ratios (ppb) averaged over WUS and EUS contributed by NO_x and reactive carbon emissions from different source regions in summer and winter during 1995–2019. Sources with small contributions are combined and shown as OTH.
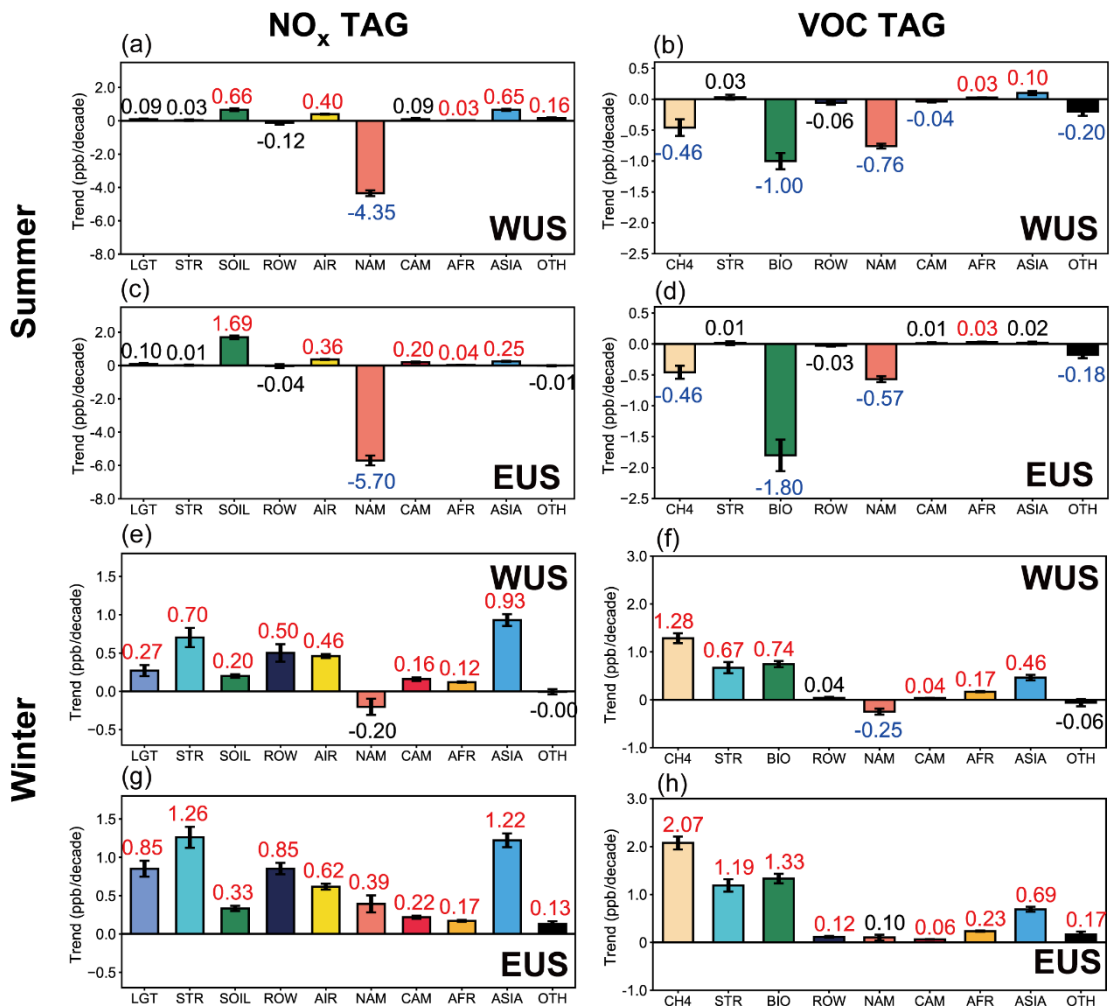
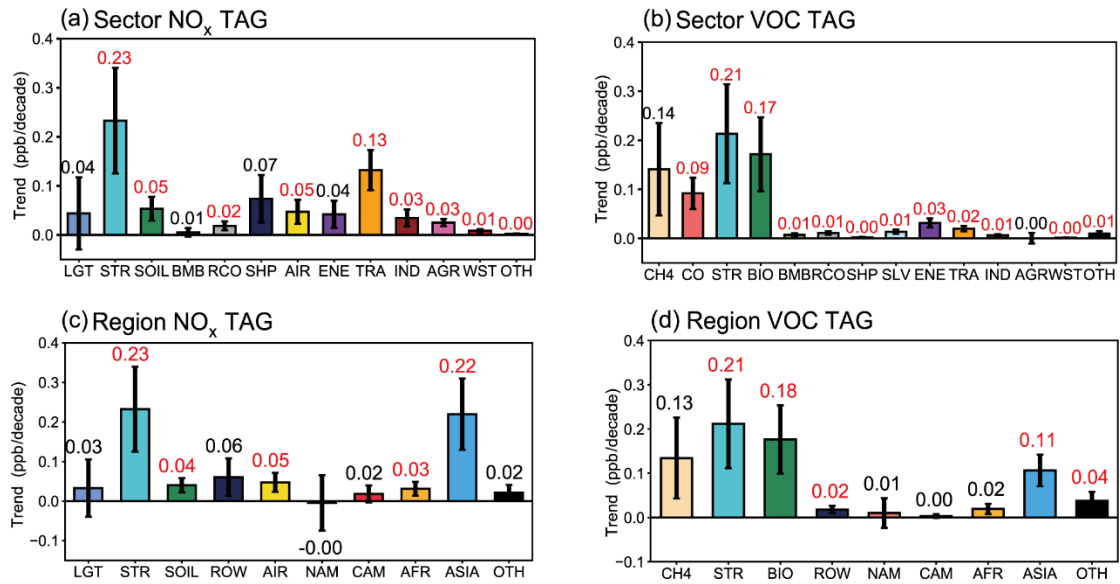**Figure 8.** Linear trends (ppb/decade) of near-surface O_3 mixing ratios in summer and winter over WUS and EUS contributed by the NO_x (left) and reactive carbon (right) emissions from various source regions (color bars). The increasing and decreasing trends marked with red and blue color numbers, respectively, indicate statistical significance with 95% confidence. Contributions from source regions EAS, SAS and SEA are combined to ASIA. Other sources having small contributions are combined and shown as OTH.
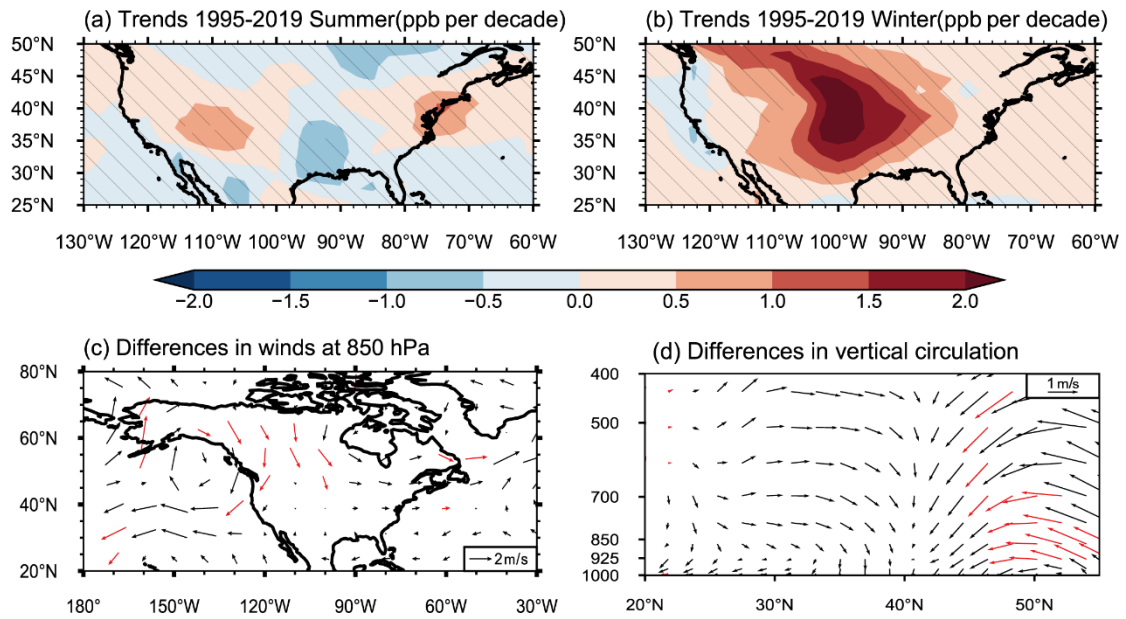
Figure 9. Linear trends (ppb/decade) of simulated (a) JJA and (b) DJF mean near-surface O_3 mixing ratios during 1995–2019. Differences between the first (1995–1999) and last (2015–2019) five years during 1995–2019 (last–first) in DJF mean (c) 850 hPa horizontal winds and (d) meridional winds and vertical velocity averaged over 90–105°W. Areas without hatches in (a) and (b) and red arrows in (c) and (d) indicate statistical significance with 95% confidence. All results are from the MET experiments.

Figure 10. Linear trends (ppb/decade) of near-surface O_3 mixing ratios in winter over the U.S, contributed by the NO_x (a,c) and reactive carbon (b,d) emissions from various source sectors (a,b) and regions (c,d). The increasing and decreasing trends marked with red and blue color numbers, respectively, indicate statistical significance with 95% confidence. Contributions from source regions EAS, SAS and SEA are combined to ASIA. Some sources having small contributions are combined and shown as OTH.